Songklanakarin J. Sci. Technol.
46 (6), 491–498, Nov. – Dec. 2024

http://www.sjst.psu.ac.th

Original Article

The 3D LiDAR scanning and speleological analysis of Saen Han Cave, Uttaradit Province, Northern Thailand

Sirinoot Teeranaew[1], Pichawut Manopkawee[1*], Rattanaporn Fongngern[1], Tadsuda Taksavasu[2], and Khomchan Promneewat[3]

[1] *Department of Geological Sciences, Faculty of Science, Chiang Mai University, Mueang, Chiang Mai, 50200 Thailand*

[2] *Department of Mining and Petroleum Engineering, Faculty of Engineering, Chiang Mai University, Mueang, Chiang Mai, 50200 Thailand*

[3] *Faculty of Civil Engineering, Graz University of Technology, Graz, 8010 Austria*

Received: 7 November 2023; Revised: 17 August 2024; Accepted: 12 September 2024

Abstract

Caves record spatial changes in landscapes and environments over millennia. Although traditional cave surveys are conducted to explore cave morphology, these techniques provide inadequate and low-resolution details on the cave features and geometry. This study conducted a 3D LiDAR scanning with the speleological investigation on the unexplored Saen Han Cave in Uttaradit province, to get a more realistic presentation of the cave characteristics. The result from cave scanning exposed the geometry of the main chamber and the connecting passageway with detailed speleothems. The lithology of the cave derived by petrographic analysis revealed that the cave was mainly composed of grainstones with distributed echinoderm fossil assemblages. These findings implied that the sedimentological environment of the limestone formation of the cave was in a marine environment. Our study highlights the combination of 3D scanning with high-resolution results and speleological analysis as a novel procedure to diagnose the cave and gain scientific insights from the cave data.

Keywords: Saen Han Cave, speleological analysis, 3D LiDAR scanning, grainstone, sedimentological environment

1. Introduction

A cave is a natural phenomenon formed by dissolving soluble rock with weakly acidic water along bedding planes, joints, and fractures. The dissolution leaves hollow spaces and passages behind with a re-deposition of cave formations or speleothems (British Geological Survey [BGS], 2023). Caves are vital to scientific research as they provide a natural index that indicates the sense of the Earth's evolution and a natural record of past climatic conditions in an area (Kambesis, 2007; White, 2007).

*Corresponding author
Email address: pichawut.m@cmu.ac.th

The shape and form of the cave are the initial outcomes of an exploration aimed at understanding the size, internal pathways, the cave's complexity, and suitable locations for surveying and collecting research data. Traditional cave surveys include determining a survey line inside the cave, labeling surveyed stations on rocks, collecting data and sketching cave features on paper, making a profile at every surveyed station, and combining all the data after explorations to create a cave map (Ginés & Ginés, 2007). However, these surveys rely on labor-intensive manual processes, outdated measurement methods, and the substantial creation of hand-drawn paper maps (Jordan, 2017). At present, although several new cave exploration approaches have been demonstrated such as vertical caving (Minton & Droms, 2019), geophysical technique (Balkaya, Göktürkler, Erhan, & Ekinci, 2012; Suranyi, Dombradi, & Leel-Ossy,

2010; Vichalai, 2019; Xi & Cui, 2021), and mathematical modeling from images (Cushing, 2012; Haruyama *et al*., 2009), the new terrestrial LiDAR (light detection and ranging) scanning is an alternative tool to enhance cave surveys that create high-resolution three-dimensional (3D) cave models quicker than manual sketches but also delivers richer information and better resolution (Šupinský, Kaňuk, Nováková, & Hochmuth, 2022; Zlot & Bosse, 2014). The models can include cross-sections from various points and capture the overall cave's geometry and details of speleothem. Furthermore, the derived information is non-subjective and scientifically reproducible (Jordan, 2017). Our study determined 3D cave models combined with speleological study by recording the components of cave morphology, speleothems, and lithologic analysis in order to generate a cave database for geotourism and to assess the paleo-formation of caves and the tectonic evolution of an area.

The study site is in the Saen Han Cave in Ban Ngom Tham, Tha Faek Sub-district, Nam Pat District, Uttaradit Province, Northern Thailand. In general, the elevation of the cave is 650 m above sea level, but it is usually flooded during the rainy season, depending on the water levels over the Sirikit Dam. The lithology of the cave falls in Carboniferous-Permian (CP) type with brown-to-brownish gray and thick-bedded sedimentary rocks, i.e., sandstone, marlstone, bioclastic limestone, and argillaceous limestone (Department of Mineral Resources [DMR], 2016). The variation in lithologies has resulted in a steep and rugged topography (Figure 1). Inside the cave, various interior cave features with numerous primary and secondary deposits and evidence of flows along with flowing water are expected to be observed. Due to the variation in geomorphic characteristics of the cave, it is crucial to integrate the latest technology by LiDAR scanning and speleological approach to document detailed 3D cave morphology, geology, and speleothems without impacting cave features.

2. Materials and Methods

The Saen Han Cave exploration processes were separated into three consecutive methods: geological field data collection, LiDAR scanning and modeling, and rock sample identification.

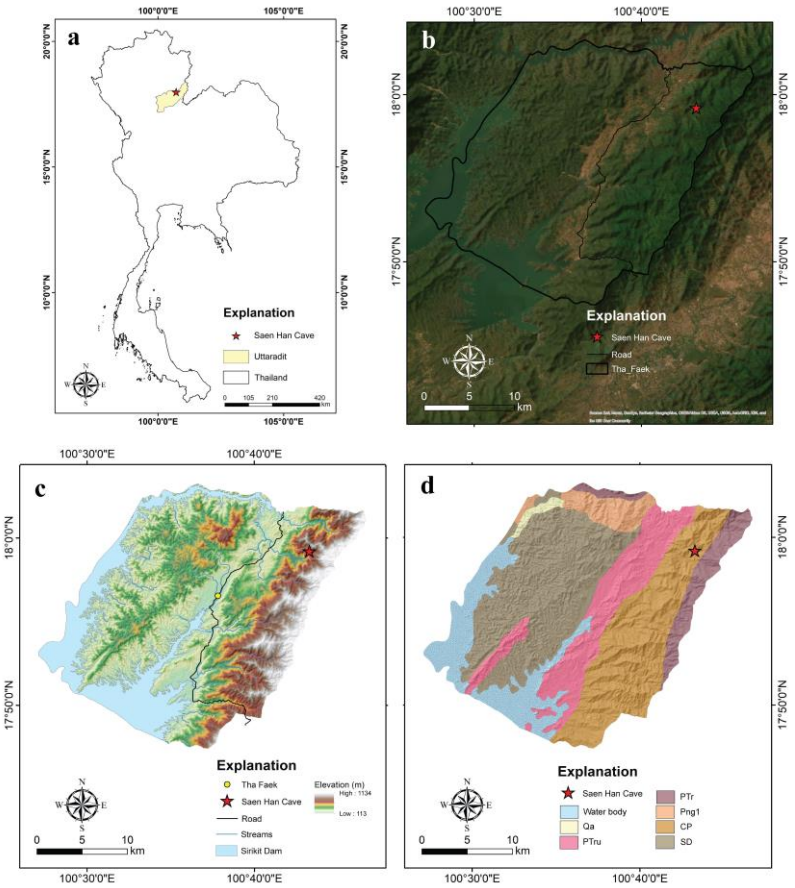

Figure 1. Geographic setting of the Saen Han Cave. (a) Location of Saen Han Cave in Tha Faek Sub-district, Nam Pat District, Uttaradit Province, Northern Thailand; (b) Saen Han Cave located in the rugged terrain with high mountains and valleys; (c) Saen Han Cave is approximately 650 m above sea level, and the water levels inside the cave depend on the water levels over the Sirikit Dam; (d) Lithologic characteristics underneath Saen Han Cave and other rock types. Abbreviations: SD. Carbonaceous and silicic phyllite, CP. Sandstone, argillaceous limestones, shale, and chert, Png1. Tuffaceous sandstone, gray-to-grayish green shale, PTr. Tuffaceous sandstone, argillaceous limestone, meta-tuff, and limestone, PTru. Ultramafic rocks, QA. Fluvial deposits and unconsolidated materials (modified from DMR, 2016)

2.1 Geological field data collection

The cave surveying process began with planning the survey line, which involved defining the linear cave from the cave entrance to the furthest point of the survey. As the cave covers a total distance of 97 m, the total distance was separated into ten surveyed stations along the survey line (Figure 2a).

Geological field data collection was started by recording the geographic coordinate location of the cave entrance and creating the survey line using a clinocompass and a portable laser rangefinder. The survey line was aligned to pass through the middle of the main chamber and the passage. Due to no signal inside the cave and the darkness, the distance travelled between stations relied on traditional cave surveys using the clinocompass, tape measure, and hand-drawn paper map. The geometry of the observed speleothems along the line was recorded and measured using a measuring tape and human scale. While surveying, at least six rock samples that were different in colours, textures, and observed fossils at the accessible study points were recorded in the description of rock samples. These rock samples were collected for petrological analysis to reveal the cave's lithological data.

2.2 LiDAR scanning and modelling

The study utilized a light detection and ranging tool (LiDAR) for detailed geological and textural surveys of the Saen Han Cave to create a 3D cave model. The LiDAR used is designed for terrestrial laser scanning technique, in which the light source is part of the device itself. The process involves the emission of light in the form of a pulsed laser from the source to a target surface and the measurement of the distance to the target surface by detecting the two-way travel time of the light (Idrees & Pradhan, 2017; Šupinský *et al*., 2022).

The LiDAR scanning technique relies on the Slamtec RP LiDAR tool, the clinocompass, and a portable laser rangefinder (Gallay *et al*., 2015). GPS cannot be applied because the satellite signals are unavailable inside the cave. Ground control points were employed at each surveyed station to align the laser scanning data and automatically tie the precise 3D cave model together. As the cave morphology and interior structure were preliminarily surveyed with the process of geological field data collection, most stations were assigned to collect data on the main chamber and speleothems (Stations 2-8). Only a few other stations were surveyed and collected for the cave passage. Thus, ten surveyed stations and ten LiDAR scanning lines at 3-9 m intervals along the survey line are sufficient to collect data from the Saen Han cave within our time limit.

As the LiDAR scanning was processed perpendicular to the survey line at 3-9 m intervals, this technique could produce numerous two-dimensional transverse profiles of the cave that were composed of a set of data points with a particular coordinate system. All acquired data from the LiDAR scanning represented the relationship between distances and angles among the points to the light source, adopting the polar coordinate system. The point cloud data were converted to Cartesian coordinates (Lippman & Rasmussen, 2018; Tian & Huang, 2021). The point cloud data in this coordinate system were shown in a reference field with x-axis and y-axis, as (x,y) coordinates. The details of scanning intervals were added as the z-axis (Dasher, 2011; Šupinský *et al*., 2022). Ultimately, these converted data were processed through the Loft surface function of computer-aided design (CAD) software (Gallay *et al*., 2015). A 3D cave model was created due to connecting profiles and surface generation (Figure 2b-c). Additionally, the geometric volume of the Saen Han cave can be estimated from the model.

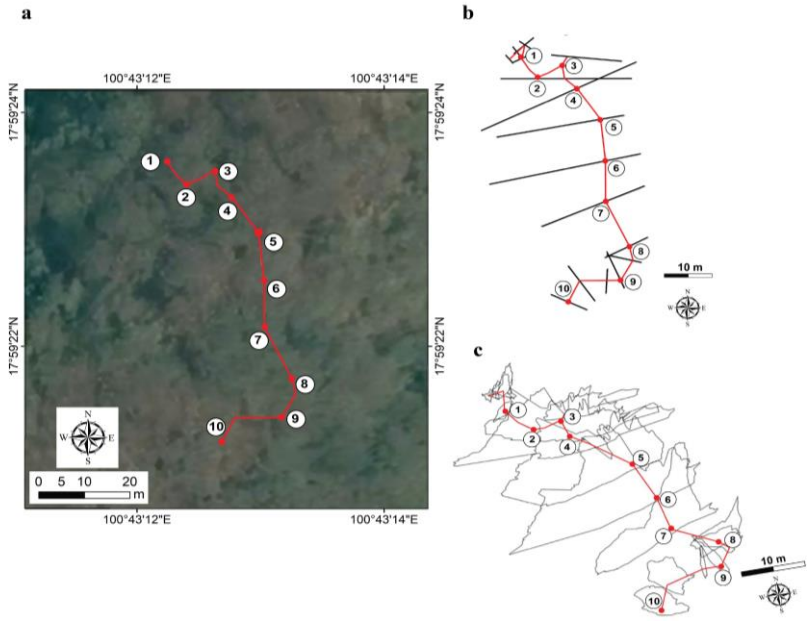

Figure 2. (a) Ten surveyed stations along a total distance of 97 m in the Saen Han Cave. (b) The top view of 17 scanning lines that cross across the survey line. (c) The perspective view exhibits the scanned profiles in each interval, showing the cave's ceiling, floor, and walls

2.3 Rock sample identification

The six rock samples collected inside the cave were identified under hand specimens to determine the rock's elemental composition, colors, textures, and physical properties. The samples were prepared into thin sections and analyzed under plane- and crossed-polarized light microscopy to assess the petrographic characteristics of the rocks. An automatic swift counter determined the amount of components by counting the components that appeared at the crosshair point for 400 points per thin section. Then, the amount of each component was calculated into its percentage.

Dunham's carbonate classification was utilized to reveal rock names and compositions based on the amount of matrix content (Dunham, 1962). This method provided additional data on cave lithology to support the 3D cave model. It informed about the sedimentological environment as a valuable clue for the formation and evolution of the Saen Han Cave.

3. Results

3.1 3D cave modeling with speleothems

The morphology and attached observed speleothems at each station were illustrated on the 3D cave model (Figure 3)**.** The observed speleothems are described as follows.

The oval-shaped cave entrance with the dimensions of 15 m in width and 2.5 m in height was assigned as Station 1. The distance from the cave entrance to Station 2 is 10 m in the direction of S10ºE. The path was a downslope of 30-35º (Figure 4a).

The survey line from Station 2 to Station 8 was inside the main chamber. At Station 2, 3-m high stalactites and a large column of 2.5 m in height with a 2.6 m circumference were located near the eastern wall of the cave. At Station 3, 3-m high stalactites and a large column were observed along the east wall in which a mass of precipitated carbonate was attached along the column's side (Figure 4b). Along the total distance of approximately 50 m between Stations 4 and Station 8, the distribution of stalactites, stalagmites, and a few columns was observed along the eastern wall of the cave. A bat cave attached to the ceiling was marked on the northwestern side of the cave. Several flowstone deposits with approximate dimensions of 90 cm in width, 70 cm in length, and 1.2 m in height were observed at Station 7. Some of these deposits presented the accumulation of carbonates in the different layered structures (20 cm thick and an average size of 30 cm) (Figure 4c). A coned stalagmite with angular holes of clast removal was noticed along the path to Station 8 (Figure 4d). The overall size of the main chamber was approximately 27.5 m wide, 54 m long, and 17.5 m high.

Station 8 was at the stepped entrance toward the cave passage. This entrance was approximately 6 m wide and 4.4 m high (Figure 5a). Along the direction S10ºE from Station 8, flowstone, rimstone, travertine, and tufa precipitated on the floor were observed (Figure 5b). The route between these two stations exposed a few weathered cave walls. The morphology of the cave walls was broader toward the upper parts connecting to the ceiling (Figure 5c). These weathered features were on average 5 m in height with a circumference of 2 m.

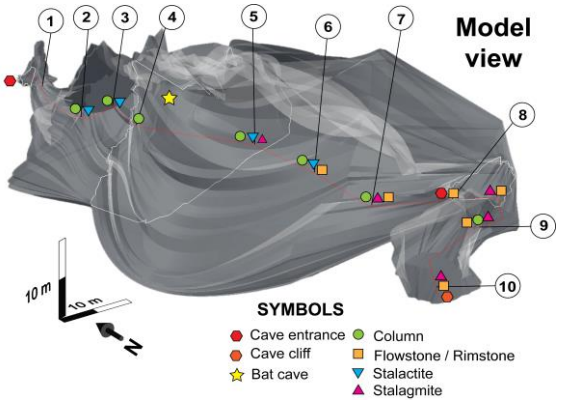

Figure 3. The profiles are stacked and surfaced to a 3D model through CAD software. The method creates the 3D model of the Saen Han Cave and exhibits the main chamber, and a passage associated with the positions of observed speleothems.

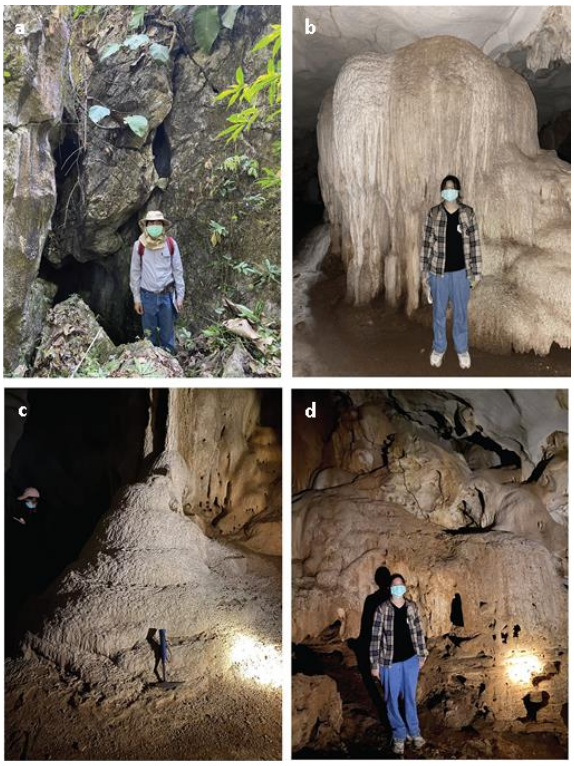

Figure 4. Examples of cave morphology and speleothems between Station 1 and Station 7. (a) The oval shape of the cave entrance with a downslope path of 30-35º. (b) A 3-m high column with a mass of precipitated carbonates. (c) Flowstone deposits. (d) Coned stalagmite with angular holes of clast removal

Station 10 was marked at the endpoint of the survey because the route was limited to a significant elevation change (approximate 15 m cave cliff) between the passage and another chamber. This station also represented a 3-to-5-m high, unmeasured circumference of the coned stalagmite (Figure 5d). Rimstones and flowstones were also found on the floor.

Figure 5. Examples of cave morphology and speleothems between Station 8 and Station 10. (a) The stepped entrance between the main chamber and the passage. (b) Rimstone on the floor. (c) The weathered cave wall has a broader morphology toward the upper part that connects to the ceiling. (d) The 3-to-5-m high, unmeasurable circumference of the coned stalagmite

3.2 Limestone analysis

The lithology of rock samples was primarily determined as a variety of carbonate rocks from hand specimen identification. These carbonate rock samples were then examined for the amount of matrix content, types of allochems, and minerals between grains under polarizing microscopy (Table 1).

Carbonate rock sample no. 1 collected at Station 2 was mainly constituted of microcrystalline calcite mud (micrite), with sparsely distributed 0.5-mm echinoderm bioclasts. This sample was considered a mudstone based on Dunham's classification (Figure 6a-b). On the other hand, carbonate rock samples no. 2, 4, 5, and 6 collected at Stations 3, 8, 9, and 10, respectively, were mainly composed of sparry carbonate cement (sparite) with a high amount of on average 0.3-0.5 mm echinoderm bioclasts and a few iron minerals. Minor fractures were filled with calcite. Based on Dunham's classification, these rock samples were determined as grainstones (Figure 6c-d). Carbonate rock sample no. 3 collected at Station 6 was totally different as it contained incomplete calcite aggregates, no carbonate grains, fossil assemblages, and other carbonate components. Thus, this limestone sample was determined to be a flowstone (Figure 6e-f).

4. Discussion

4.1 3D cave modeling

The study demonstrates the integration of the geological field data collection, LiDAR scanning and modeling, and rock sample classification to create the 3D, high-resolution model of the Saen Han cave with details of speleothems, cave structures, and rock description. Ten LiDAR scanning stations provide sufficient point cloud data to make a 3D cave model (Figure 3) that presents the large main chamber and open space covered by clay left after flooding and dying on the floor and the walls. The field data collection also represents a collection of gigantic stalagmites, stalactites, and columns along the cave's east side, while the cave's northwest side and the ceiling are attached to a large bat cave. The cave's passage exposes many enormous columns with rimstones, flowstones, travertine, and tufa. However, the cave survey is limited to the cliff between the passage and another chamber in the lower elevation.

The 2D cave maps that are released from numerous studies in many places around the world illustrate a flat cave morphology on paper with required visualization for the cave morphology. The 2D maps do not provide the ability to observe the geometry and speleothems with different angles and perspectives. Moreover, making a 2D cave map is time-consuming and expensive, as it requires transferring data collection and in-cave sketches into software and digitizing those data and sketches into cave cartography. The LiDAR technology is the latest exploration method that can reveal details of cave geometry based on patterns of georeferenced data points. The number of data points typically depends on the availability of surfaces or targets that the probing light beam can reach. In this work, the time spent scanning the narrow and large passages was identical.

Table 1. Classification of rock samples based on the percentage of matrix, carbonate content, and other components (Dunham, 1962)

Sample number (no.)	Matrix		Allochems			Calcite vein	Iron (Fe)	Quartz	Sum (%)	Rock sample name
	Micrite	Sparite	Echino-derms	Fasulinid	Other					
1	60.30	24.50	2.50	-	1.00	11.70	-	-	100	mudstone
2	27.80	39.50	25.00	-	0.50	4.50	2.50	0.20	100	grainstone
3	Unable to count calcite components									flowstone
4	64.30	19.70	1.80	-	0.20	14.00	-	-	100	mudstone
5	20.00	74.50	2.50	-	-	3.00	-	-	100	grainstone
6	29.30	56.40	6.00	0.20	1.30	3.50	3.30	-	100	grainstone

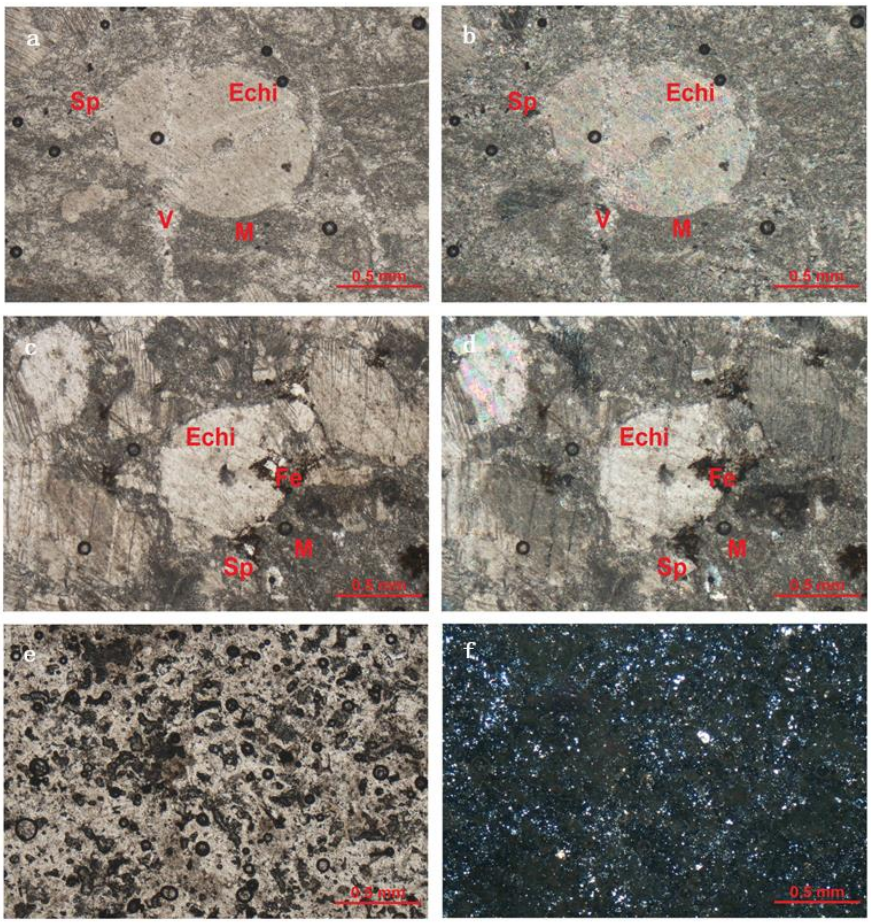

Figure 6. Examples of thin sections of carbonate rocks under a plane light (left) and a crossed polarized light (right). (a-b) Carbonate rock sample no. 1 is considered a mudstone. (c-d) Carbonate rock sample no. 6 is considered a grainstone. (e-f) Carbonate rock sample no. 3 is considered a flowstone. Abbreviations: M. Micrite, Sp. Sparite, Echi. Echinoderms, V. Calcite vein, and Fe. Iron

Compared to the 2D cave maps derived from traditional cave surveys, the 3D cave model with geological field data provides the overall macro-scale morphology and internal textures of the cave walls, floors, and ceilings and detailed features, including speleothems like flowstones, curtains, stalactites, and stalagmites. Our tool used in the cave survey is one of the LiDAR Simultaneous Localization and Mapping (LiDAR SLAM) collections that can create a map in various environments while concurrently determining their position within the map. The generation of 3D point clouds from the LiDAR SLAM systems can deliver a precise map and instant localization across diverse applications such as autonomous vehicles, robotics, and indoor mapping for navigation (Debeunne & Vivet, 2020). The LiDAR SLAM is efficient in directly collecting smoother 3D surface of the interior of the cave, although a cave map derived from LiDAR technology takes longer duration of the cave survey, more processing and computational costs, with a time-consuming process, and a huge amount of memory required for detail collection (Cosso, Ferrando, & Orlando, 2014; Jordan, 2017).

Compared with a conventional hand-sketched map, the LiDAR SLAM can capture cave morphology in the form of a point cloud in a high spatial resolution, generate 3D cave models, and provide more detail of the cave, speleothems, and speleological activities. The 3D cave model is better for visualization of the complex cave plan and incline views with the interpretation of the important cave features and elevation changes inside the cave. The derived 3D cave model can be further transformed into 3D printing, interactive web-based visualization using open-source tools for point clouds, and caving simulations and virtual tours, which serve as educational tools for individuals who are unable to visit caves in person. This process can be an alternative way to present the speleological exploration data and provides a new quick method to produce the three-dimensional model as a reference map for other further uses.

4.2 Implications for evolution of the Saen Han Cave

The combination of hand specimen identification and the plane- and crossed-polarized light microscopy reveals that most collected limestone samples are grainstones based on a large amount of micrite, echinoderm assemblages, and calcite fill-in fractures (Dunham, 1962). The appearance of micrite in the limestone indicates chemical and biological precipitations from seawater in the calm lagoon or quiet-water environments where the wave base is in the deeper ocean (Abd El-Moghny & Afifi, 2022; Yousef *et al.*, 2023).

However, echinoderms typically live on the ocean floor in various marine environments. They are abundant in shallow to deep ocean habitats and are commonly found on rocky shores, coral reefs, and sandy bottom oceans (Sprinkle & Guensburg, 1995). Hence, these types of limestone suggest that the paleo-environmental condition of the limestone is likely to form in a range of shallow to deep marine environments.

Based on the findings of the sedimentological environments of the Saen Han Cave, our results imply that geologic evolution and the sedimentary process of the cave's limestone formed in the marine environment during the late Carboniferous and Permian (DMR, 2021). Our research reveals the sedimentological environment of the cave and supports the tectonic evolution of Sundaland, represented by Metcalfe (2002) and Morley (2002). The Sibumasu plate moved northward from the Gondwana landmass in the southern hemisphere to a warm climate-lower latitude by the middle to late Permian. It was the time period that the carbonate and sediment formed within a marine environment on the passive continental margin before the collision of the Sibumasu block with Sukhothai terrain and the close of southeastern paleo-Tethys in late Permian-early Triassic (Bunopas, 1981; Feng, Yang, Shen, Chonglakmani, & Malila, 2008; Metcalfe, 2011; Wakita & Metcalfe, 2005). The collision of those tectonic blocks caused a progressive uplift and a spatial change in a range of carbonate facies with the emergence of terrigenous sediment deposits (Charusiri, Daorerk, Archibald, Hisada, & Ampaiwan, 2002). This time period during the tectonic uplift might be the beginning of the formation of the cave chamber and speleothems.

5. Conclusions

This study focused on cave exploration in the Saen Han Cave, Uttaradit province, Northern Thailand, using the integration of LiDAR scanning and speleological study to generate a 3D cave model with a detailed description of cave morphology and speleothems. A geological field data survey was conducted to collect cave morphology, structures, and speleothems along the survey line. These field data were combined with the 3D model generated by LiDAR technology to present cave morphology and geometry in three-dimensional views. The 3D cave model exposes the macro-scale main chamber connected to the passage. A collection of speleothems derived from the field survey was added to the 3D cave model. Cave lithology is mostly grainstone and implies that the paleo-sedimentological environment ranges from shallow to deep marine environments. These limestone samples are related to the carbonate formation before the collision of plates and the progressive uplift of interacting tectonic blocks. Overall, the study demonstrates a high-resolution 3D model with details of features inside the Saen Han Cave using the latest methods of speleological investigation with LiDAR technology. This research can be used as a reference model and method for exploring other caves elsewhere.

Acknowledgements

This work was supported by the Department of Geological Sciences, Faculty of Science, Department of Mining and Petroleum Engineering, Faculty of Engineering, Chiang Mai University, and Thoranee Krasib Co., Ltd. We thank Mr. Chanawut Suksabai, Mr. Sathit Kanthata, Mr. Piyapong Obchoi, Ms. Mesinee Maneechedtha, and Ms. Yanisa Chaingam for their advice on cave exploration and field assistance. Appreciation is expressed to Mr. Viwat Teeranaew, the head of the Huai Phueng Forest Watershed Management Unit 11 (Phitsanulok), and all workers for their field assistance, logistics, navigations, guidance, and meals and refreshments. We acknowledge anonymous reviewers' critical comments and suggestions to improve the manuscript significantly.

References

Abd El-Moghny, M. W., & Afifi, A. A. (2022). Microfacies analysis and depositional environments of the Middle Eocene (Bartonian) Qurn Formation along Qattamiya-Ain Sokhna district, Egypt. *Carbonates Evaporites, 37,* 18. doi:10.1007/s13146-022-00762-9

Balkaya, C., Göktürkler, G., Erhan, Z., & Ekinci, Y. L. (2012). Exploration for a cave by magnetic and electrical resistivity surveys: Ayvacık Sinkhole example, Bozdağ, İzmir (western Turkey). *Geophysics, 77,* B135–B146. doi:10.1190/geo2011-0290.1

British Geological Survey. (2023). *Caves and Karst*. Retrieved from https://www2.bgs.ac.uk/mendips/caveskarst/karst_1.htm

Bunopas, S. (1981). *Paleogeographic history of western Thailand and adjacent parts of South-East Asia. A plate tectonic interpretation* (Doctoral thesis, Victoria University of Wellington, Wellington, New Zealand). Retrieved from https://cmu.on.worldcat.org/oclc/10334515

Charusiri, P., Daorerk, V., Archibald, D., Hisada, & K., Ampaiwan, T. (2002). Geotectonic evolution of Thailand: A new synthesis. *Journal of the Geological Society of Thailand, 1*, 1–20.

Cosso, T., Ferrando, I., & Orlando, A. (2014). Surveying and mapping a cave using 3D laser scanner: the open challenge with free and open source software. *The International Achieves of the Photogrammetry Remote Sensing and Spatial Information Sciences, 5*, 181-186. doi:10.5194/isprsarchives-XL-5-181-2014

Cushing, G. E. (2012). Candidate cave entrances on Mars. *Journal of Cave and Karst Studies, 74*, 33–47. doi:10.4311/2010EX0167R

Dasher, G. R. (2011). *On station*: *A complete handbook for surveying and mapping cave*. Huntsville, Alabama: National Speleological Society.

Debeunne, C., & Vivet, D. (2020). A review of visual-LiDAR fusion based simultaneous lactation and mapping. *Sensors, 20*, 2068. doi:10.3390/s20072068

Department of Mineral Resources. (2016). *Geological map scale 1:250,000 NE 47–11, Changwat Uttaradit*. Retrieved from https://oer.learn.in.th/search_detail/result/14922

Department of Mineral Resources. (2021). *Caves and karst of Thailand*. Retrieved from https://www.thailandcaves.shepton.org.uk/cave-karst-book

Dunham, R. J. (1962). Classification of carbonate rocks according to depositional texture**.** In W. E. Ham (ed.), *Classification of Carbonate Rocks* (pp**.** 108–121)**.** Tulsa, OK: AAPG (American Association of Petroleum Geologists).

Feng, Q., Yang, W. Q., Shen, S. Y., Chonglakmani, C., & Malila, K. (2008). The Permian seamount stratigraphy sequence in Chiang Mai, North Thailand and its tectogeographic significance. *Science in China Series D*: *Earth Sciences, 51*, 1768-1775. doi:10.1007/s11430-008-0121-5

Gallay, M., Kaňuk, J., Hochmuth, Z., Meneely, J. D., Hofierka, J., & Sedlák, V. (2015). Large-scale and high resolution 3-D cave mapping by terrestrial laser scanning: A case study of the Domica cave, Slovakia. *International Journal of Speleology, 44*, 277-291. doi:10.5038/1827-806X.44.3.6

Ginés, A., & Ginés, J. (2007). Eogenetic karst, glacioeustatic cave pools and anchialine environments on Mallorca Island: A discussion of coastal speleogenesis. *International Journal of Speleology, 36*, 57–67. doi:10.5038/1827-806X.36.2.1

Haruyama, J., Hioki, K., Shirao, M., Morota, T., Hiesinger, H., van der Bogert, C.H., . . . Pieters, C.M. (2009). Possible lunar lava tube skylight observed 500 by SELENE cameras. *Geophysical Research Letter, 36*, L21206. doi:10.1029/2009GL040635

Idrees, M. O., & Pradhan, B. (2017). Geostructural stability assessment of cave using rock surface discontinuity extracted from terrestrial laser scanning point cloud. *Journal of Rock Mechanics and Geotechnical Engineering, 10*, 534-544. doi:10.1016/j.jrmge.2017.11.011

Jordan, J. H. (2017). *Modeling Ozark Caves with structure-from-motion photogrammetry*: *an assessment of stand-alone photogrammetry for 3-dimensional cave survey* (Master thesis, University of Arkansas, AR). Retrieved from https://core.ac.uk/download/pdf/127621674.pdf

Kambesis, P. (2007). The importance of cave exploration to scientific research. *Journal of Cave and Karst Studies, 69*, 46–58**.**

Lippman, D., & Rasmussen, M. (2018). *Precalculus*: *An Investigation of Functions* (2nd ed). Retrieved from https://www.opentextbookstore.com/precalc/

Metcalfe, I. (2002). Permian tectonic framework and paleogeography of SE Asia. *Journal of Asian Earth Sciences, 20*, 551–566. doi:10.1016/S1367-9120(02)00022-6

Metcalfe, I. (2011). Paleozoic-Mesozoic history of SE Asia. *Geological Society London Special Publications, 355*, 7–35. doi:10.1144/SP355.2

Morley, C. (2002). A tectonic model for the Tertiary evolution of strike-slip faults and rift basins in SE Asia. *Tectonophysics, 347*, 189–215. doi:10.1016/S0040-1951(02)00061-6

Minton, M., & Droms, Y. (2019). Exploration of caves-vertical caving techniques**.** In W.B. White, D.C. Culver & T. Pipan (Eds), *Encyclopedia of Caves* (*3rd edition*, pp**.** 420–425). Cambridge, MA: Academic Press.

Sprinkle, J., & Guensburg, T. E. (1995). Origin of Echinoderms in the Paleozoic Evolutionary Fauna: The Role of Substrates. *Palaios, 10*, 437–453. doi:10.2307/3515046

Šupinský, J., Kaňuk, J., Nováková, M., & Hochmuth, Z. (2022). LiDAR point clouds processing for large-scale cave mapping: A case study of the Majko dome in the Domica cave. *Journal of Maps, 18*, 268–275. doi:10.1080/17445647.2022.2035270

Suranyi, G., Dombradi, E., & Leel-Ossy, S. (2010). Contribution of geophysical techniques to the exploration of the Molnar Janos Cave (Budapest, Hungary). *Acta Carsologica, 39*, 565–576. doi:10.3986/ac.v39i3.84

Tian, Z., & Huang, Y. (2021). Transformation between polar and rectangular coordinates of stiffness and dampness parameters in hydrodynamic journal bearings. *Friction, 9*, 201–206. doi:10.1007/s40544-019-0328-9

Vichalai, C. (2019). Geophysics under stressed: A case study of Tham Luang Nang Non Cave. *RMUTSB Academic Journal, 7*, 247–258**.**

Wakita, K., & Metcalfe, I. (2005). Ocean plate stratigraphy in East and Southeast Asia. *Journal of Asian Earth Sciences, 24*, 679–702. doi:10.1016/j.jseaes.2004.04.004

White, W. B. (2007). Cave sediments and paleoclimate. *Journal of Cave and Karst Studies, 69*, 76–93.

Xi, J., & Cui, D. (2021). Research on comprehensive exploration technology of underground soil karst cave. IOP Conference Series. *Earth and Environmental Science, 660*, 012012. doi:10.1088/1755-1315/660/1/012012

Yousef, I., Morozov, V. P., Kolchugin, A. N., Sudakov, V., Idrisov, I., & Leontev, A. (2023). Microfacies analysis and depositional environment of the Upper Devonian Dankovo-Lebedyansky sediments, Tatarstan, Volga-Ural Basin, Russia. *Petroleum Research, 8*, 244–255. doi:10.1016/j.ptlrs.2022.07.003

Zlot, R., & Bosse, M. (2014). Three-dimensional mobile mapping of caves. *Journal of Cave and Karst Studies, 76*, 191-206. doi:10.4311/2012EX0287